



HAL
open science

Selecting Generalized Continuum Theories for Nonlinear Periodic Solids Based on the Instabilities of the Underlying Microstructure

Christelle Combescure

► **To cite this version:**

Christelle Combescure. Selecting Generalized Continuum Theories for Nonlinear Periodic Solids Based on the Instabilities of the Underlying Microstructure. *Journal of Elasticity*, inPress, 10.1007/s10659-022-09949-6 . hal-03859192

HAL Id: hal-03859192

<https://ubs.hal.science/hal-03859192>

Submitted on 6 Dec 2022

HAL is a multi-disciplinary open access archive for the deposit and dissemination of scientific research documents, whether they are published or not. The documents may come from teaching and research institutions in France or abroad, or from public or private research centers.

L'archive ouverte pluridisciplinaire **HAL**, est destinée au dépôt et à la diffusion de documents scientifiques de niveau recherche, publiés ou non, émanant des établissements d'enseignement et de recherche français ou étrangers, des laboratoires publics ou privés.

Selecting generalized continuum theories for nonlinear periodic solids based on the instabilities of the underlying microstructure

Christelle Combescure^{1,2*}

^{1*}CREC Saint-Cyr, Académie Militaire de Saint-Cyr Coetquidan, F-56380, Guer, France.

²IRDL, Univ. Bretagne Sud, UMR CNRS 6027, F-56100, Lorient, France.

Corresponding author(s). E-mail(s):
c.combescure@st-cyr.terre-net.defense.gouv.fr;

Abstract

In the context of architected materials, it has been observed that both long-wavelength instabilities leading possibly to localization and short-wavelength instabilities leading to the apparition of a deformation pattern could occur. This work proposes for the first time a comparison of the ability of two families of higher order equivalent media, namely strain-gradient and micromorphic media, to capture both patterning and long-wavelength macroscopic instabilities in those materials. The studied architected material consists in a simple one-dimensional arrangement of non-linear springs, thus allowing for analytical or nearly analytical treatment of the problem, avoiding any uncertainties or imprecisions coming from a numerical method. A numerical solution of the problem is then used to compare the post-buckling prediction of both models. The study concludes that, micromorphic media are the appropriate choice of equivalent continuum models to employ when dealing with the possibility of patterning inside a structured medium, but if long-wavelength global instability is of interest, a strain-gradient type equivalent medium is well suited.

1 Introduction

Due to their interesting and sometimes even exotic mechanical properties, architected materials are more and more studied nowadays. As defined in [1–3], architected materials consists in an arrangement of material on at least three length scales: the microscopic scale, describing the constitutive material(s) composition, the macroscopic scale, describing the structure composed by the architected material and the mesoscopic scale(s) describing the constitutive material(s) arrangement in space.

The behavior of such materials when submitted to compressive loading has been extensively studied and experiments have led to the conclusion that, when architected materials have a periodic mesoscale arrangement, meaning that they are composed of periodic unit cells, two types of instabilities can occur in those materials: (i) long-wavelength instabilities, that take place at the macroscopic scale and can lead to either global buckling or localization and (ii) short-wavelength "cell-commensurate" instabilities that creates a deformation pattern at the mesoscopic scale. These two types of instabilities are illustrated on Fig.1 (a) (b) alongside with a localized deformation (c). Localization can happen after a long-wavelength instability and in the case presented in Fig.1.c, a shortwavelength instability appeared first, followed by a long-wavelength instability that lead to a localization as explained in [4].

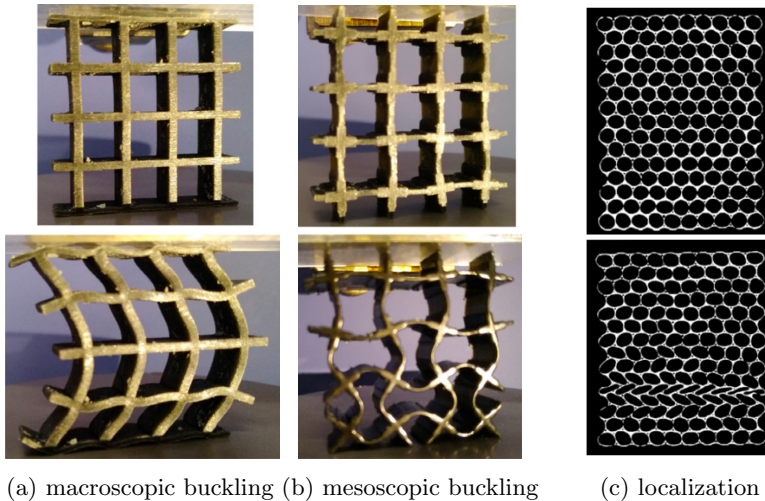


Fig. 1: Various types of instabilities observed in architected materials. (a) and (b) from [5] and (c) from [6]

When dealing with architected materials, it is common to have a scale separation between all scales, meaning that the number of mesoscopic cells in the whole structure can be large. As a consequence, the computation of

the non-linear behavior of these structures when submitted to compressive loadings can lead to excessively large amount of time if all the mesoscopic cells have to be taken into account. It is thus quite natural to try to build an equivalent continuum medium to the architected material, able to capture its essential behaviors, in order to reduce the computation time. Moreover, as presented in the coming paragraph, it has been shown that generalized media are to consider if one wants to capture instabilities in architected materials.

Before reviewing the scientific literature on the generalized media for short and long-wavelength instabilities, it can be useful to present the two main families of generalized media [7–11]. A scheme from [12] and adapted in Fig.2 presents the two families that stem from a classical Cauchy medium when trying to generalize the kinematics: the higher-order gradient family and the additional degrees-of-freedom (DOF) family. From the left to the right on the scheme Fig.2, local rotational degrees-of-freedom then local stretch degrees-of-freedom are added to the kinematics. For additional DOF continua these extensions are independent DOF, while for higher-order gradient continua they are controlled by higher-order gradients of the displacement field. This construction is, in essence, very similar to the well-known construction of the Timoshenko and Euler-Bernoulli beams. In a Timoshenko beam, the rotational DOF is independent of the transverse displacement which places this model in the additional DOF family. The Euler-Bernoulli beam links the rotational DOF with the transverse displacement using a derivative, thus placing it in the higher-order gradient family. In the literature concerning generalized continua, several models have been built using these concepts: the Cosserat model [13] consists in adding only local rotational degrees of freedom to the kinematic field while the micromorphic medium [14, 15] adds not only a local rotational DOF but also a local stretch DOF. Both models belong to the additional DOF family that will be named, in the remainder of this paper the *micromorphic family*. On the other hand, what is commonly known as the Koiter model [16] is a model built using the antisymmetric part of the displacement gradient as the rotational degree of freedom while the strain-gradient model [8] is built using the first gradient of the strain as the stretch degree of freedom, thus placing naturally these models in the higher-order gradient family, named, in the remainder of this paper the *strain-gradient family*. These models can be linked to their counterpart in the micromorphic family using kinematical constraints [11, 12]. Of course these two families can be combined to create micromorphic strain-gradient models if necessary.

In the context of instabilities appearing in periodic architected materials, pioneer article by [17] studied the ability of a strain-gradient model to capture long wavelength instabilities and localization appearing in a periodic arrangement of one-dimensional springs. This model, built by a Taylor expansion of the mesoscopic displacement, appeared to be perfectly able to capture the macroscopic long-wavelength instability and the subsequent localization phenomenon that appeared. No mention of the possible short-wavelength

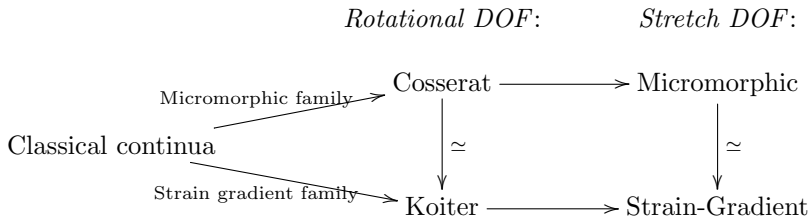


Fig. 2: Basic extensions of a classical continuum. Adapted from [12].

buckling was made in this article. In [18], authors propose a quasi-continuum model based also on strain-gradient in order to capture both long and short wavelength instabilities appearing in a periodic arrangement of atoms linked by non-linear interatomic potentials. The conclusion is that the quasi-continuum media can capture some sort of short-wavelength instability, but it appears that the buckling threshold is not appropriately captured by the model. Finally, [19] have recently proposed a micromorphic computational homogenization procedure to capture patterning, meaning short-wavelength instabilities.

Based on the observation that, in architected materials, both short and long-wavelength instabilities can occur, and that both micromorphic and strain-gradient media have been proposed in the literature to capture such behaviors, it is of interest in this study to compare the ability of these two types of generalized media to capture each type of instability on a very simple problem. As a consequence, the example of a periodic arrangement of non-linear springs, as presented in Fig.3 below has been proposed. This model will be studied analytically and two generalized media, one micromorphic and one strain-gradient, will be derived from the discrete model. While the strain-gradient medium has already been built in [17], it is the first time a micromorphic medium is constructed on such model. Moreover, a numerical analysis is performed on the model in order to compare, for the first time, the ability of each model to capture post-buckling behavior including localization.

2 Discrete system

2.1 Setting

Consider a one-dimensional structure composed of initially equally spaced nodes connected by non-linear elastic springs, clamped at one end and submitted to an end force at the other end. The node spacing is denoted by b and the total length of the structure is $L = Nb$ where $N \gg 1$. The structure thus has a total number of $N + 1$ nodes. A typical node n is connected to its adjacent

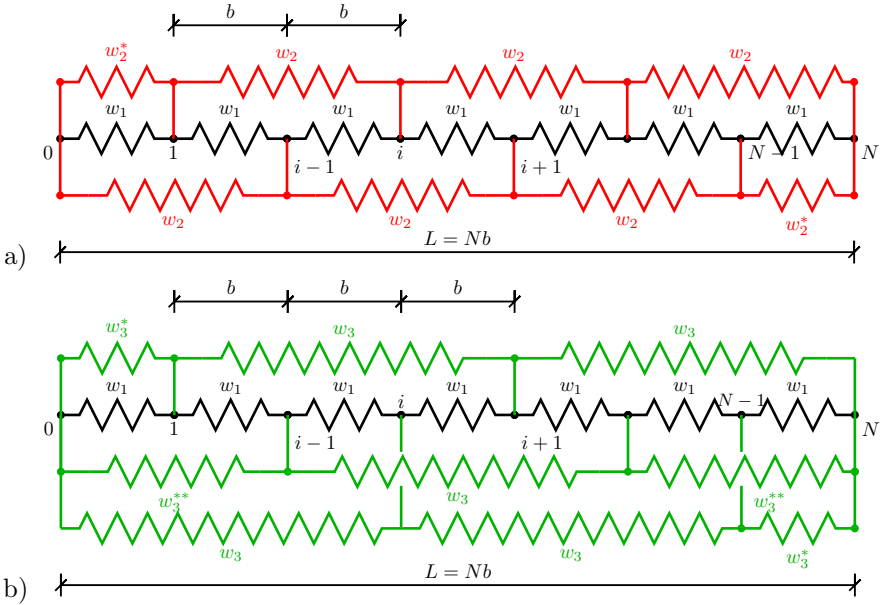


Fig. 3: 1D arrangement of non-linear springs with connections to (a) next-to-neighbor node ($q = 2$) and (b) next-to-next-to-neighbor node ($q = 3$). Black, red and green springs have different internal energies represented by the letter w indexed by a number. At the boundaries of the systems, the internal energy w_2^* , w_3^* and w_3^{**} of boundary springs are adapted in order to ensure uniform initial equilibrium state across the system's length.

nodes m with possibility to connect to nodes further than the immediate neighboring node as displayed in Fig.3 where a connection to the next-to-neighbor node is presented in (a) and a connection to the second-to-next-to-neighbor node presented in (b). As such, an integer q indicates the maximum number of neighboring nodes to which each node is connected on each side.

The strain ϵ_p in a spring of length pb ($1 \leq p \leq q$) attached to node n is given by Eq.1:

$$\epsilon_n^{p+} = \frac{u_{n+p} - u_n}{pb} \quad \text{or} \quad \epsilon_n^{p-} = \frac{u_n - u_{n-p}}{pb}. \quad (1)$$

The stored energy density in a spring of length pb is $w_p(\epsilon^p)$. A special choice has been made for the stiffness of the boundary springs since, at both ends, the springs connecting nodes further than the immediate neighbors have to be adjusted in order to ensure a uniform solution prior to instability. This choice resulted in the addition of boundary springs with stored energy w_2^* , w_3^* or w_3^{**1} in Fig.3 linking first and last boundary nodes to their first or second neighbors. The stored energy density of the complete discrete structure, denoted W , equals half of the energy of all springs connected to an interior node n divided

¹ $w_2^*(\epsilon) = w_2(\epsilon)$, $w_3^*(\epsilon) = w_3(\epsilon/3)$ and $w_3^{**}(\epsilon) = w_3(2\epsilon/3)$

by nodal spacing b , as presented in Eq.2:

$$W(u_0, u_1, \dots, u_N) = \frac{1}{2} \sum_{n=0}^{n=N} \sum_{p=1}^q p [w_p(\epsilon_p^{n+}) + w_p(\epsilon_p^{n-})]. \quad (2)$$

The total energy of the system is then defined by:

$$\mathcal{E}(u_0, u_1, \dots, u_N) = W(u_0, u_1, \dots, u_N) - \frac{1}{Nb} F u_N, \quad (3)$$

where F is the force exerted at the end node N necessary to induce the displacement u_N . The system is then submitted to an end force F at node N that can be compressive or tensile depending on its sign.

The discrete system is considered to be at equilibrium when the derivative of this energy with respect to the displacement of node n is null for all nodes n inside the system. This condition give rises to the following system of differential equations and boundary conditions:

$$\frac{\partial W}{\partial u_n} = 0 \quad \forall n \in [0, N-1] \quad ; \quad \frac{\partial W}{\partial u_N} = \frac{F}{Nb} \quad ; \quad u_0 = 0 \quad (4)$$

A solution of the system of equilibrium equations (Eq.4) is called an equilibrium state and noted $\overset{0}{\mathbf{u}}$, where \mathbf{u} is the vector of nodal displacements (u_0, u_1, \dots, u_N) . In order to access stability of this equilibrium state, perturbations $\delta\mathbf{u}$ of the equilibrium state are introduced and the positive definiteness of the quadratic part of the energy expansion under such perturbations is studied:

$$\left. \frac{\partial}{\partial \eta} \left(\frac{\partial W(\overset{0}{\mathbf{u}} + \eta \delta\mathbf{u})}{\partial u_n} \right) \right|_{\eta=0} > 0 \quad \forall \delta\mathbf{u} \in \mathbb{R}^n \quad (5)$$

The equilibrium state $\overset{0}{\mathbf{u}}$ is said to be stable whenever Eq.5 is true and unstable otherwise. In a discrete system, this is equivalent to studying the positive definiteness of the second derivative of the total energy with respect to the displacement vector.

For the sake of simplicity, we will study, in this paper, only the cases $q = 2$ depicted in Fig.3a) and $q = 3$ where $p = 2$ is forbidden depicted in Fig.3b). As for the non-linear stored energy per unit length for one spring, it will be taken equal to the one proposed in the Type A model of [17]:

$$w_p(\epsilon) = \frac{1}{2} K_p \epsilon^2 - \frac{1}{4} M_p \epsilon^4 + \frac{1}{6} N_p \epsilon^6, \quad (6)$$

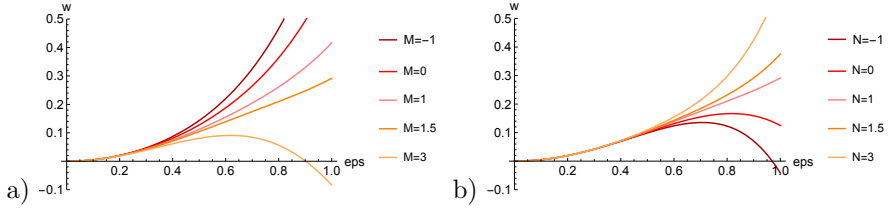


Fig. 4: Representative plots of energy function w as a function of deformation ϵ for a) several values of quartic parameter M , when other parameters K and N are set to 1 and b) several values of sextic parameter N , when other parameters K and M are set to 1 and 1.5, respectively.

where K_p , M_p and N_p are *stiffness*-like coefficients for the spring and are then considered to be intrinsic constants. One recognizes, in the quadratic term, the usual stored energy function for linear springs $w_p(\epsilon) = 1/2 K_p \epsilon^2$. Thus K_p has to be positive in order to ensure realistic springs. The attentive reader would notice that this non-linear stored energy being only built out of even order powers of deformation, the proposed system behaves symmetrically in tension or compression. Representative plots of the energy function w_p proposed in Eq.6 is proposed in Fig.4 for various values of stiffness parameters M and N . One could notice that some parameters might lead to a non-convex energy.

2.2 Stability Analysis

The discrete system, in the cases $q = 2$ and $q = 3$ with $w_2 = 0$, using the stored energy function presented in Eq.6, presents an equilibrium equation for a given inner node n of the form:

$$\begin{aligned}
 0 = & b^4 K_1 ((u_n - u_{n+1}) - (u_{n-1} - u_n)) - b^2 M_1 ((u_n - u_{n+1})^3 - (u_{n-1} - u_n)^3) \\
 & + N_1 ((u_n - u_{n+1})^5 - (u_{n-1} - u_n)^5) \\
 & + b^4 K_q \left(\frac{u_n - u_{n+q}}{q} - \frac{u_{n-q} - u_n}{q} \right) - b^2 M_q \left(\left(\frac{u_n - u_{n+q}}{q} \right)^3 - \left(\frac{u_{n-q} - u_n}{q} \right)^3 \right) \\
 & + N_q \left(\left(\frac{u_n - u_{n+q}}{q} \right)^5 - \left(\frac{u_{n-q} - u_n}{q} \right)^5 \right)
 \end{aligned} \tag{7}$$

A trivial solution to this equation is given by $u_n = u_{n+p} \quad \forall n \in [0, N] \quad \forall -q \leq p \leq q$, leading to a uniform displacement of all the nodes corresponding to a global translation that is forbidden by the clamped condition at the left end node 0.

Another solution would be $u_n - u_{n+1} = u_{n-1} - u_n$ & $u_n - u_{n+q} = u_{n-q} - u_n \quad \forall n \in [0, N]$ which corresponds to uniform strain $\epsilon_p^{n+} = \epsilon_p^{n-} = \epsilon \quad \forall n \in$

8 *Selecting generalized continuum theories based on instabilities*

$[0, N]$ $\forall -q \leq p \leq q$ of the discrete system. This solution will be named *principal solution* and further noted $\overset{0}{\mathbf{u}}$. Of interest in this study will be the stability of this principal solution $\overset{0}{\mathbf{u}}$.

Following the methodology proposed in [4, 20, 21], we will use the Bloch-waves analysis (also termed the phonon or Floquet method) to study stability of the principal solution. This method consists in perturbing the studied displacement solution by plane-waves such that the perturbation of node $n+p$ is related to the perturbation of node n by:

$$\delta u_{n+p} = \delta u_n e^{2i\pi kpb}, \quad (8)$$

where k is the normalized spatial wavenumber corresponding to the imposed plane-wave. k sets the periodicity of the imposed plane wave in the reciprocal space meaning that a wavenumber $k = 1/2b$ corresponds to a periodicity of $2b$ in the direct space thus spreads on two springs. The periodic states of perturbation proposed by the Bloch-wave analysis create a null mean deformation state and as such, correspond to stability analysis with respect to a displacement control system. As such, the following stability analysis establishes a necessary condition for the system's stability.

We are then left with determining the conditions for Eq.5 to be satisfied, in order to ensure stability of the principal solution $\overset{0}{\mathbf{u}}$ under the Bloch-wave perturbation Eq.8. . This leads to the following equation:

$$W_{,nn-2} e^{-4i\pi kb} + W_{,nn+2} e^{4i\pi kb} + W_{,nn-1} e^{-2i\pi kb} + W_{,nn+1} e^{2i\pi kb} + W_{,nn} > 0. \quad (9)$$

where $W_{,nm} = \frac{\partial^2 W}{\partial u_n \partial u_m} \Big|_u$ with $m = n \pm q$ corresponds to the only non-zero terms in the quadratic part of the energy expansion (5). The complete expression for these terms are:

$$\begin{aligned} W_{,nn} &= \frac{1}{b^2} \left[K_1 - 3M_1 \epsilon^2 + 5N_1 \epsilon^4 + \frac{1}{q} (K_q - 3M_q \epsilon^2 + 5N_q \epsilon^4) \right] \\ W_{,nn-1} &= \frac{-1}{2b^2} (K_1 - 3M_1 \epsilon^2 + 5N_1 \epsilon^4) = W_{,nn+1} \\ W_{,nn-q} &= \frac{-1}{2qb^2} (K_q - 3M_q \epsilon^2 + 5N_q \epsilon^4) = W_{,nn+q}. \end{aligned} \quad (10)$$

Using expressions for $W_{,nm}$ terms defined in Eq.10 and semi-angle formulæ, Eq.9 simplifies to:

$$\sin^2(\pi kb) g_1(\epsilon) + \frac{\sin^2(q\pi kb)}{q} g_q(\epsilon) > 0 \quad q = 2or3 \quad (11)$$

where g_i stiffness functions, defined as $g_i(\epsilon) = K_i - 3M_i \epsilon^2 + 5N_i \epsilon^4$ $i \in \mathbb{N}$, have been introduced to further simplify the expressions.

This latter Eq.11 resembles the one presented in Eq.7 of [18] as it presents a

quadratic term of \sin .

The stability of the system is satisfied for a given ϵ^0 as long as for all values of k , Eq.11 holds true. It appears that the function of k appearing in this equation presents extrema for $kb = 1/q + \alpha$, $q = 2, 3$ and $\alpha \in \mathbb{Z}$ and $k \rightarrow 0$. As a consequence, the only unstable wavelengths are:

- the short-wavelength instability associated with wavelength $k = 1/qb$ corresponding to a periodic instability at the scale of $q = 2$ or 3 springs of length b , respectively to the studied system. This instability will appear at global strain ϵ^0 solution of $g_1(\epsilon^0) = 0$ ² for both cases $q = 2$ and $q = 3$. This type of instability was named "commensurate" in [18]³;
- the long-wavelength instability corresponding to the case of $k \rightarrow 0$ (acoustic branch) appearing when the global strain ϵ^0 is such that $g_1(\epsilon^0) + qg_q(\epsilon^0) = 0$ for both cases $q = 2$ and $q = 3$.

Fig.5 presents the commensurate buckling modes of both cases $q = 2$ and $q = 3$. The original period tripling mode appearing for the $q = 3$ mode is presented for the first time and merely consists in the first spring to reduce in size while the third one increases when the middle spring stays undeformed.

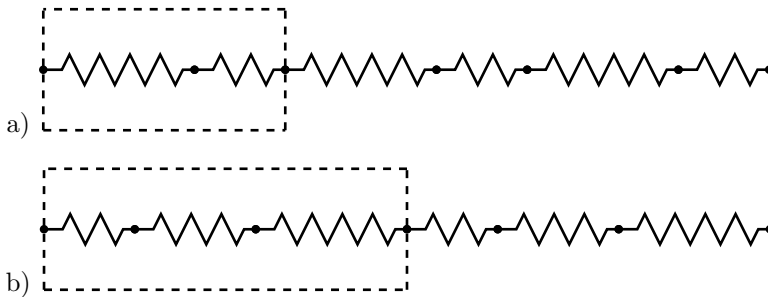


Fig. 5: Commensurate modes for both cases a) $q = 2$ and b) $q = 3$ represented only on the shortest springs connecting direct neighboring nodes. The mode periodicity is emphasized by dashed borders.

Using g_1 and g_q , a stability diagram can be established in the plane of these two "parameters". Then, since these parameters are actually functions that depends on the global applied strain ϵ , the loading path followed by these functions as ϵ increases can be plotted. On Fig.6, the stable region is represented in blue with orange and green borders corresponding to short

²corresponding to $\epsilon^2 = \frac{3M_1}{10N_1} \pm \frac{1}{10N_1} \sqrt{9M_1^2 - 20K_1N_1}$ with $20N_1K_1 < 9M_1^2$

³in the case $q = 3$ a mode on 2 springs is also possible but will appear at global strain ϵ^0 solution of $g_1(\epsilon^0) + g_3(\epsilon^0)/3 = 0$ which will always lead to greater values of ϵ^0 than condition $g_1(\epsilon^0) = 0$, as shown in Fig.6.

and long-wavelength instability criteria, respectively. This graph also presents examples of loading paths leading to long-wavelength instability (green), short-wavelength instability (orange) or no instability (blue). All these paths start in the stable region and evolve to cross either the green, the orange or no border. If no border is crossed, the path remains stable for all values of deformations. The parameters chosen for these paths make them cross the border twice so that they recover stability after a trip in the unstable regime⁴; this feature is not compulsory and it is possible to design systems that would remain unstable all along.

The parameters chosen to plot the green, orange and blue paths are the following:

- long-wavelength unstable path $K_1 = 1, K_2 = 1, M_1 = -1, M_2 = 3, N_1 = 1, N_2 = 1$
- short-wavelength unstable path $K_1 = 1, K_2 = 1, M_1 = 2, M_2 = 1, N_1 = 1, N_2 = 1$
- stable path $K_1 = 1, K_2 = 1, M_1 = 1, M_2 = 1.6, N_1 = 1, N_2 = 1$

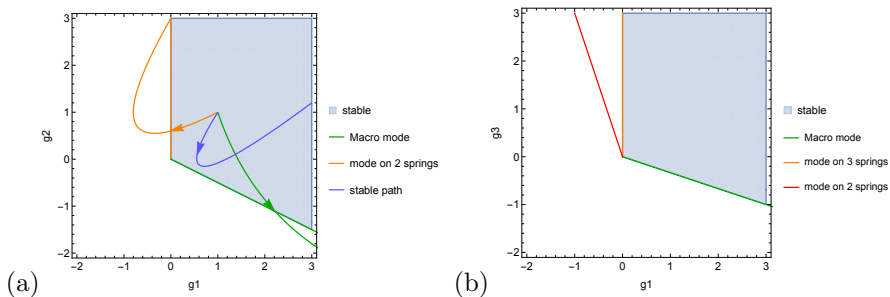


Fig. 6: Stability diagrams for the discrete model with (a) $q = 2$ and (b) $q = 3$. Region of stability is shaded in blue. Orange and green borders to this blue stability region correspond to criteria for short and long-wavelength instabilities, respectively. In plain colored lines with arrows are plotted examples of loading paths leading to long-wavelength instability (green), short-wavelength instability (orange) and no instability (blue). Parameters for these paths are stated in the text.

The question can now be posed of which instability will appear first depending on the system's stiffness parameters K_i, M_i and $N_i, i = 1, 2, 3$. One can notice that there are only three possible stability regimes: always stable, short-wavelength unstable or long-wavelength unstable. An interesting and new result presented here is that the conditions for these regimes to exist are independent of deformation values and only depends on the system's stiffness parameters K_i, M_i and $N_i, i = 1, 2, 3$. These conditions are presented below

⁴The return of stability appears for the green path out of the bounds of the graph that has been zoomed on the zone of interest

only for the case $q = 2$, for the sake of clarity. They depend only on four logical expressions. The negation of a logical expression will be noted with an overline, for instance $\text{cond } 0 : K_1 + 3M_1 > 0 \Rightarrow \overline{\text{cond } 0} : K_1 + 3M_1 \leq 0$.

- conditions for a stable path for all imposed global strains:

$$\underbrace{M_1 < \frac{2}{3}\sqrt{5K_1N_1}}_{\text{cond 1}} \quad \& \quad \underbrace{M_2 < \frac{-M_1}{2} + \frac{\sqrt{5}}{3}\sqrt{(K_1 + 2K_2)(N_1 + 2N_2)}}_{\text{cond 2}}$$

These conditions derive from the fact that, in order to be fully stable for all imposed strains, one has to ensure that $g_1(\epsilon) > 0$ and $g_1(\epsilon) + 2g_2(\epsilon) > 0 \quad \forall \epsilon$. Both equations correspond to second order polynomial equations in terms of ϵ^2 which are ensured to be always positive if and only if the discriminant of these equations is negative.

Now, choosing for instance $K_1 = K_2 = N_1 = N_2 = 1$, cond 1 imposes $M_1 < \frac{2\sqrt{5}}{3} \approx 1.49$. Picking $M_1 = 1$, cond 2 leads to $M_2 < \frac{-1}{2} + \sqrt{5} \approx 1.736$, for example $M_2 = 1.6$. The loading path corresponding to this choice of stiffness parameters is plotted in plain blue line in Fig.6.

- conditions for a short-wavelength instability to appear first along the principal path:

$$\overline{\text{cond } 1} \quad \& \quad \underbrace{6M_2 + \frac{|K_2N_1 - K_1N_2|}{K_1N_1}\sqrt{9M_1^2 - 20K_1N_1}}_{\text{cond 3}} < 3M_1 \left(\frac{K_2}{K_1} + \frac{N_2}{N_1} \right)$$

In the case considered here one wants to ensure that short-wavelength instability will appear before long-wavelength instability. Thus one wants that $g_1(\epsilon) + 2g_2(\epsilon) > 0$ when $g_1(\epsilon) = 0$ for the same ϵ . Using the derived conditions and choosing, for instance, $K_1 = K_2 = N_1 = N_2 = 1$, $\overline{\text{cond } 1}$ implies $M_1 > \frac{2\sqrt{5}}{3} \approx 1.49$. Picking $M_1 = 2$, cond 3 leads to $M_2 < M_1 = 2$; for example $M_2 = 1$. The loading path corresponding to this choice of stiffness parameters is plotted in plain orange line in Fig.6.

- conditions for a long-wavelength instability appearing first along the principal path:

$$\underbrace{M_1 \leq \frac{2}{3}(K_2N_1 + K_1(N_1 + N_2))\sqrt{\frac{5}{(K_1 + 2K_2)(N_1 + 2N_2)}}}_{\text{cond 4}} \quad \& \quad \overline{\text{cond } 2}$$

or
 $\overline{\text{cond } 4} \quad \& \quad \overline{\text{cond } 3}$

These conditions have been derived by considering that one must have $g_1(\epsilon^0) > 0$ when $g_1(\epsilon^0) + 2g_2(\epsilon^0) > 0$ for the same ϵ^0 in order to ensure that long-wavelength instability appears before short-wavelength instability. For instance, choosing $K_1 = K_2 = N_1 = N_2 = 1$, cond 4 implies $M_1 \leq \frac{2\sqrt{5}}{3} \approx 1.49$. Picking $M_1 = -1$, $\overline{\text{cond } 2}$ leads to $M_2 \geq \frac{-1}{2} + \sqrt{5} \approx 2.736$; for example $M_2 = 3$. The loading path corresponding to this choice of stiffness parameters is plotted in plain green line in Fig.6.

Additionally, the two previously described instabilities can appear simultaneously whenever $g_1(\epsilon^0) = g_2(\epsilon^0)$, but this condition has a very low probability of appearance in real systems due to the presence of unavoidable defects.

In order to be realistic, the structure has to be stable under null applied strain for all wavelength thus leading to the conditions $K_1 + 2K_2 > 0$ & $K_1 > 0$ which are both automatically satisfied when K_1 and K_2 are taken to be positive, as specified in the problem setting section.

3 Homogenization

Of interest in this study is the comparison of the micromorphic-type and the strain-gradient-type homogenized media in their ability to capture short and long-wavelength instabilities of non-linear spring assemblies. This section details the derivation of both equivalent continuum energies on the case $q = 2$. The case $q = 3$ leads to qualitatively the same results.

3.1 Strain-gradient equivalent medium

This part follows the strain-gradient energy derivation proposed in [17]. It proposes a rewriting of the presented derivation of equations and the last paragraph extends [17] conclusions to the case of local instabilities that had not been studied in their paper.

The strain-gradient homogenization strategy is based on a Taylor series expansion of the displacement continuous function $u(x)$ that is assumed to coincide with all equilibrium discrete displacements u_n at nodal points $x_n = nb$ corresponding to node n . As such, using Eq.1, the strains ϵ_n^{p+} and ϵ_n^{p-} in all the non-linear springs affecting node n equilibrium can be expressed as in Eq.12 where the following simplified notation is used $u_{,x} = \frac{du(x)}{dx}$:

$$\begin{aligned} \epsilon_n^{p+}(x) &= \frac{u_{n+p} - u_n}{pb} = u_{,x} + \frac{1}{2}pbu_{,xx} + \frac{1}{6}(pb)^2u_{,xxx} + \dots \\ \epsilon_n^{p-}(x) &= \frac{u_n - u_{n-p}}{pb} = u_{,x} - \frac{1}{2}pbu_{,xx} + \frac{1}{6}(pb)^2u_{,xxx} - \dots \end{aligned} \quad (12)$$

Introducing this decomposition into the stored energy density of the discrete structure Eq.2, one gets the following expression for the strain-gradient

stored energy, where the discrete sum is naturally replaced by an integral over the length $L = Nb$ of the system:

$$W^s(u, x) = \int_0^L w_1(u, x) + 2w_2(u, x) - \frac{b^2}{24} [(w_1''(u, x) + 8w_2''(u, x)) (u, x)_{,xx}^2] + O(b^4) dx \quad (13)$$

Thus, using the Type A stored energy function Eq.6, the homogenized strain-gradient macroscopic stored energy is then:

$$W^s(u, x) = \int_0^L \underbrace{u, x(x)^2 \frac{K_1 + 2K_2}{2} - u, x(x)^4 \frac{M_1 + 2M_2}{4} + u, x(x)^6 \frac{N_1 + 2N_2}{6}}_{\mathcal{E}(u, x(x))} + \underbrace{(u, x(x))^2 \frac{b^2}{2} \frac{1}{12} [-(K_1 + 8K_2) + 3(M_1 + 8M_2)u, x(x)^2 - 5(N_1 + 8N_2)u, x(x)^4]}_{h(u, x(x))} dx. \quad (14)$$

The equilibrium equation corresponding to this stored energy is found by differentiating it with respect to admissible displacements. This leads, using generalized Euler-Lagrange equations, to Eq.15:

$$\mathcal{E}'(u, x(x)) - b^2 \left(u, xxx(x) h(u, x(x)) + \frac{(u, xx(x))^2}{2} h'(u, x(x)) \right) = F \quad (15)$$

where F is the external applied force exerted at the end of the structure and $(\cdot)'$ stands for a derivation with respect to macroscopic strain $E(x) = u, x$. A trivial solution to this equation is $u, x(x) = \overset{0}{E} \forall x \in [0, L]$. This corresponds to the principal path of our discrete problem with homogeneous mesoscopic strain $\overset{0}{\epsilon}$.

In order to study the stability of this principal equilibrium state, one must examine the positive definiteness of the second variation of the homogenized strain-gradient macroscopic energy regarding all admissible displacement δu and evaluated along the principal path:

$$W^s, uu(\overset{0}{u}) = \int_0^L \mathcal{E}''(\overset{0}{E})(\delta u, x)^2 + b^2 h(\overset{0}{E})(\delta u, xx)^2 dx \quad (16)$$

where $\overset{0}{u}$ is the uniform displacement creating the macroscopic strain $\overset{0}{E}$. One can use the following functions satisfying the admissible to zero boundary

conditions $\delta u(0) = \delta u(L) = 0$:

$$\delta u(x) = \sqrt{\frac{2}{L}} \sum_{m=1}^{\infty} \delta u_m \sin\left(\frac{m\pi x}{L}\right). \quad (17)$$

Again, the periodic states of perturbation proposed here create a null mean deformation state and as such, correspond to stability analysis with respect to a displacement control system. As such, the following stability analysis establishes a necessary condition for the system's stability.

The admissible to zero functions yield the stability condition:

$$\sum_{m=1}^{\infty} \left[\mathcal{E}''(\overset{0}{E}) + b^2 \left(\frac{m\pi}{L}\right)^2 h(\overset{0}{E}) \right] \left(\frac{m\pi}{L} \delta u_m\right)^2 > 0. \quad (18)$$

As explained in [17], this stability condition is satisfied as long as $\mathcal{E}''(\overset{0}{E}) + \left(\frac{bm\pi}{L}\right)^2 h(\overset{0}{E}) > 0$. Using the Type A stored energy function Eq.6 the stability condition of Eq.18 takes the following form:

$$\begin{aligned} & (K_1 + 2K_2) - 3(M_1 + 2M_2)(\overset{0}{E})^2 + 5(N_1 + 2N_2)(\overset{0}{E})^4 \\ & + \frac{(bm\pi)^2}{12L^2} \left[-(K_1 + 8K_2) + 3(M_1 + 8M_2)(\overset{0}{E})^2 - 5(N_1 + 8N_2)(\overset{0}{E})^4 \right] > 0 \end{aligned} \quad (19)$$

Loss of stability corresponds to Eq.19 equal to zero, it will thus depend on the value of non-dimensional parameter b/L and integer m as follows:

- the first condition arising when studying instability corresponds to the long-wavelength condition with $m = 0$: $\underbrace{K_1 - 3M_1 E^2 + 5N_1 E^4 + 2(K_2 - 3M_2 E^2 + 5N_2 E^4)}_{g_1(E) + 2g_2(E)} = 0$,
- the second condition corresponds to $m = \frac{\sqrt{3}L}{b\pi}$ and $\underbrace{K_1 - 3E^2 M_1 + 5E^4 N_1}_{g_1(E)} = 0$. But m has to be rational for the boundary conditions to be respected and b/L is fixed by the ratio of microscopic to macroscopic lengths. As a consequence, there is little to no chance for this second condition to be respected and thus, the short-wavelength instability will be miscaptured by the strain-gradient equivalent continuum.

Another way to see this is to remark that, if $\mathcal{E}''(\overset{0}{E})$ stays positive for all macroscopic strains $\overset{0}{E}$, the system does not reach a global maximum in the principal path $\overset{0}{u}(F)$ and thus the strain-gradient model loses its pertinence since it has been built to detect a loss of stability after a global maximum.

3.2 Micromorphic equivalent medium

The stability analysis of the discrete system has shown that only two unstable modes could occur in the case $q = 2$: a short-wavelength period-doubling instability and a long-wavelength instability. It is of interest in this study to derive *homogenized* models that would be able to capture both modes. The studied system being periodic of period b , the micromorphic homogenization strategy consists in writing the springs node displacements according to the Cauchy-Born hypothesis [22], corresponding to the description of the displacement field as the sum of a homogeneous displacement Ex and a periodic displacement, named *shift*, s :

$$u(x) = Ex + s(x), \quad (20)$$

where E is the applied macroscopic strain supposed to be known, x is the continuous equivalent to the position of the node and $s(x)$ the periodic shift (unknown), function of the continuous node position. This hypothesis is similar to the one usually applied in the periodic homogenization process.

Given that the stability analysis of the discrete system uncovered the possibility for a period-doubling instability to occur in the $q = 2$ system, the homogenization will take place on a unit-cell comprising two adjacent nodes n and $n + 1$, thus working on a total length of two periods: $2b$ ⁵. In order to prevent uniform translations, node n is considered to be fixed: $u_n = 0$. With these assumptions, the strains of each spring connected to the studied nodes n and $n + 1$ can be computed from Eq.1:

$$\epsilon_n^{1+} = E + \frac{s(x)}{b}; \quad \epsilon_n^{1-} = \epsilon_{n+1}^{1+} = E - \frac{s(x)}{b}; \quad \epsilon_n^{2+} = \epsilon_n^{2-} = \epsilon_{n+1}^{2+} = \epsilon_{n+1}^{2-} = E \quad (21)$$

Using the Type A stored energy function Eq.6 along with the strain expressions derived in Eq.21 and injecting those into the stored energy of the structure composed of 2 nodes ($N=1$) Eq.2 leads to the following homogenized internal energy:

$$\begin{aligned} W^m(u_{,x}(x), s(x)) = & \int_0^L u_{,x}^2(x) \frac{K_1 + 2K_2}{2} - u_{,x}^4(x) \frac{M_1 + 2M_2}{4} + u_{,x}^6(x) \frac{N_1 + 2N_2}{6} \\ & + \frac{K_1 - 3u_{,x}^2(x)M_1 + 5u_{,x}^4(x)N_1}{2} \left(\frac{s(x)}{b} \right)^2 \\ & - \frac{M_1 - 10u_{,x}^2(x)N_1}{4} \left(\frac{s(x)}{b} \right)^4 + \frac{N_1}{6} \left(\frac{s(x)}{b} \right)^6 dx \quad (22) \end{aligned}$$

The attentive reader could notice in this last expression that the homogenized internal micromorphic energy when the shift is null $W^m(u_{,x}, 0)$ is equal to the term gathered in $\mathcal{E}(u_{,x})$ – the first order term – of the homogenized

⁵If one wanted to study the $q = 3$ system, a total length of three periods would be considered for the construction of the micromorphic equivalent medium

strain gradient energy Eq.14. Additionally, the displacement shift $s(x)$ appears to be always associated with microscopic length b as $s(x)/b$; this term can be called the "deformation shift" and examples later on will explain its physical interpretation.

The homogenized internal energy Eq.22 now depends on two state variables: the macroscopic displacement $u(x)$ and the deformation shift $s(x)/b$. In order to obtain the equilibrium of such system, one need to use generalized Euler-Lagrange equations for several functions of a single variable. Thus, differentiating this internal energy with respect to the macroscopic displacement, gives rises to the macroscopic equilibrium of the structure where a loading term F corresponding to the external applied force exerted at the end of the structure appears (Eq.23).

$$u_{,x} (K_1 + 2K_2 - u_{,x}^2(M_1 + 2M_2) + u_{,x}^4(N_1 + 2N_2)) + (-3M_1 + 10N_1 u_{,x}^2) u_{,x} \left(\frac{s}{b}\right)^2 + 5N_1 u_{,x} \left(\frac{s}{b}\right)^4 = F \quad (23)$$

Additionally, differentiating this energy with respect to the deformation shift $s(x)/b$ leads to the equation for the internal equilibrium of the periodic unit cell:

$$\frac{s(x)}{b} \left[(K_1 - 3u_{,x}^2 M_1 + 5u_{,x}^4 N_1) - (M_1 - 10u_{,x}^2 N_1) \left(\frac{s(x)}{b}\right)^2 + N_1 \left(\frac{s(x)}{b}\right)^4 \right] = 0, \quad (24)$$

which admits several solutions. The trivial solution $s(x) = 0$ describes an homogeneous strain of the structure and corresponds to the principal path. Eq.24 corresponds to the evolution law of state variable deformation shift $s(x)/b$ with respect to macroscopic deformation $E = u_{,x}$.

The stability of the principal path can be studied by looking at the second variation of the stored energy with respect to both state variables evaluated along the principal path (meaning that $s = 0$):

$$\det \begin{bmatrix} W_{,uu} & W_{,us} \\ W_{,us} & W_{,ss} \end{bmatrix} \Big|_{u=u_0, s=0} > 0$$

When the determinant of this matrix becomes null under admissible variations, the stability of the system is lost. One can use the same admissible functions as determined in Eq.17⁶ and thus ends up with a loss of stability when one of

⁶Again, the periodic states of perturbation proposed here create a null mean deformation state and as such, correspond to stability analysis with respect to a displacement control system.

the two conditions listed in Eq.25 is satisfied:

$$\underbrace{K_1 - 3M_1E^2 + 5N_1E^4}_{g_1(E)} = 0 \text{ or } \underbrace{K_1 - 3M_1E^2 + 5N_1E^4 + 2(K_2 - 3M_2E^2 + 5N_2E^4)}_{g_1(E)+2g_2(E)} = 0 \quad (25)$$

One can then recognize immediately in these equations the two conditions $g_1(\epsilon) = 0$ and $g_1(\epsilon) + 2g_2(\epsilon) = 0$ established in subsection 2.2.

As a consequence, the homogenized model using the deformation shift as additional state variable has the ability to capture both short-wavelength and long-wavelength instabilities.

4 Numerical study

Strain-gradient models have an internal length, and as such have been proven to be numerically efficient to capture localization phenomena as underlined in [17]. It is thus of interest to compare the numerical efficiency of both models in cases where short-wavelength instabilities appear but also in a case with a long-wavelength instability followed by a localization. These two cases are presented below in the case of the $q = 2$ system. They correspond to the orange and green cases presented in the discrete analysis section and are related to the following set of parameters: $K_1 = K_2 = N_1 = N_2 = 1$ and $M_1 = 2$, $M_2 = 1$ for the short wavelength instability and $M_1 = 1$, $M_2 = 2$ for the long wavelength instability. They will be modeled on the full discrete system including all the springs and using both equivalent media applied to the boundary value problem with adequate boundary values. The computations have been carried out using a custom home-made bifurcation and branch-following software [23, 24] for the discrete and micromorphic models and using software AUTO-07p [25] for the strain-gradient model.

The problem of interest for this numerical study is an arrangement of 40 springs connecting direct neighboring nodes associated with internal energy $w_1(\epsilon^1)$ and 39 springs connecting next-to neighbor springs associated with internal energy $w_2(\epsilon^2)$. In order to ensure a regular constant strain principal solution, the boundary next-to neighbor springs are in fact connected to their direct neighbor and associated with an internal energy $w_2(\epsilon^1)$ as represented in Fig.3. This arrangement of springs is considered to be clamped on the left end and submitted to an end force F associated with end displacement Δ at the other end.

When using the micromorphic equivalent medium, and internal length has to be set corresponding to the ratio between the microscopic to the macroscopic length. In this model, it has been chosen as $b/L = 1/40$ in accordance with the number of springs in the discrete model. A finite difference scheme has been employed with 40 elements. This number of elements has been increased or decreased without changing the displayed results.

4.1 Short-wavelength instability

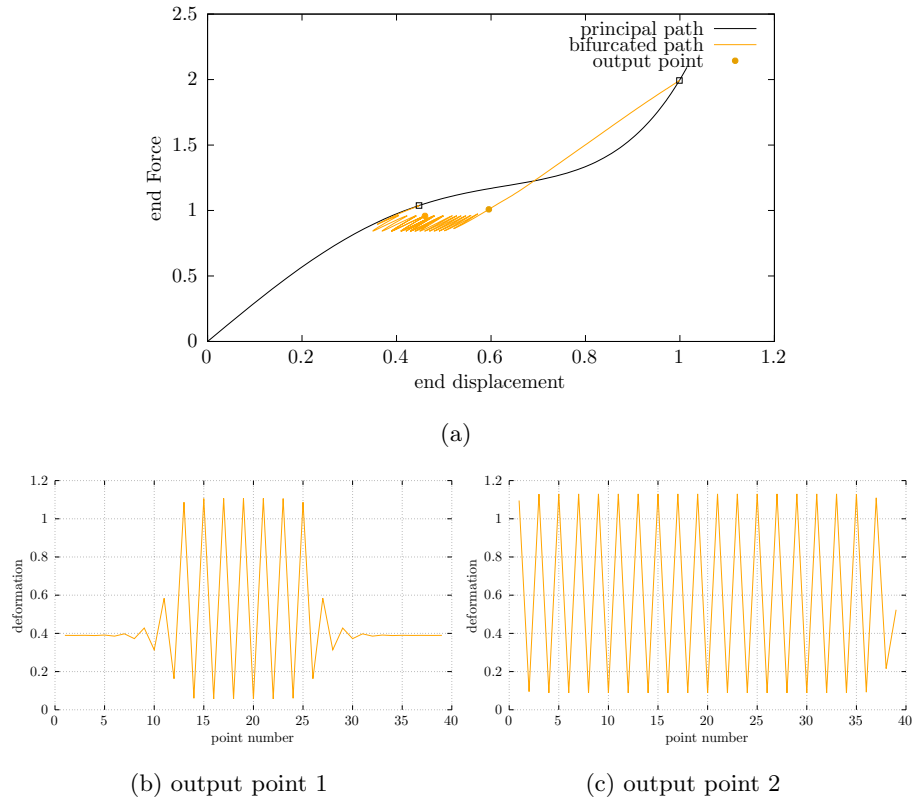


Fig. 7: Numerical results of computation on the discrete system where a short wavelength instability appears first along the principal path. (a) End force-displacement graph with principal path in black and first bifurcated branch in orange. Empty squares mark the location of bifurcation points and the plain circles are the computation points for which bifurcated modes are outputted. (b) state of deformation across the discrete system at the first output point on the bifurcated branch and (c) state of deformation across the discrete system at the second output point on the bifurcated branch.

Internal energy model parameters are chosen to be $K_1 = K_2 = 1$, $N_1 = N_2 = 1$ and $M_1 = 2$, $M_2 = 1$ so that the system should display a short-wavelength instability that spans over two nodes, as explained in the discrete analysis section.

Results corresponding to the numerical computation of the problem on the discrete system are displayed in Fig.7. The systems shows a monotonic principal branch (Fig.7a) in plain black line with a bifurcation point appearing at

$(\Delta_\epsilon, F) = (0.44773, 1.03815)$. From that point, a bifurcated branch in plain orange line emerges that displays wide oscillations corresponding to propagation of the alternate mode across the springs (Fig.7b) to finally reach the entire length of the system Fig.7c. The bifurcated branch appears to be unstable up to the end of the oscillations where it stabilizes. The predicted short-wavelength instability is thus confirmed and appropriately spreads across two nodes as represented by the alternate values of deformation on each node. The system has a discrepancy in terms of deformation, which loses uniformity near the ends, corresponding to the fact that it is not infinite.

When using the micromorphic equivalent medium, the principal path is appropriately captured and the bifurcation point corresponds to $(\Delta_E, F) = (0.447214, 1.0375355)$ with relative error of 10^{-3} on the displacement and of $6 \cdot 10^{-4}$ on the force value. No oscillations are observed on the bifurcated branch which directly corresponds to a uniform internal shift across the system's length. This bifurcated branch appears to be unstable on its downward part and stabilizes after its minimum. Fig.8a presents the end force-displacement curve for the micromorphic equivalent medium. In transparent plain orange line is displayed the results on the discrete model for comparison. A very good agreement between the discrete and the micromorphic model can be observed on this curve. This agreement can also be observed when comparing the values of deformation and deformation shift ($= s/b$) coming from the micromorphic medium to the values of the local deformation from the discrete model displayed on Fig.8b. Indeed, the micromorphic deformation E corresponds to the mean deformation of the bifurcated mode while the micromorphic deformation shift s/b is the amplitude of the discrete mode oscillations.

Now, when using the strain-gradient equivalent medium, the principal path is also appropriately captured. Several bifurcation points appear on this branch including one before the bifurcation point of interest. The closest bifurcation point to the one found by the discrete model appears at $(\Delta_E, F) = (0.449357, 1.0400949)$ with relative error of $3 \cdot 10^{-3}$ on the displacement and of $1.8 \cdot 10^{-3}$ on the force value, meaning that the error is three times higher than for the micromorphic medium. Additionally, the bifurcated branch differs from the discrete bifurcated branch and does not converge all the way.

From this first numerical study of a short-wavelength bifurcating system, it appears that the micromorphic medium is more precise to capture the onset of short-wavelength bifurcation and more accurate in the prediction of the bifurcated branch than the strain-gradient medium which cannot converge all the way along the bifurcated branch. This confirms the conclusions drawn after the analytical analysis carried out in the homogenization section: when dealing with patterning instabilities, a micromorphic equivalent medium is appropriate to capture these instabilities.

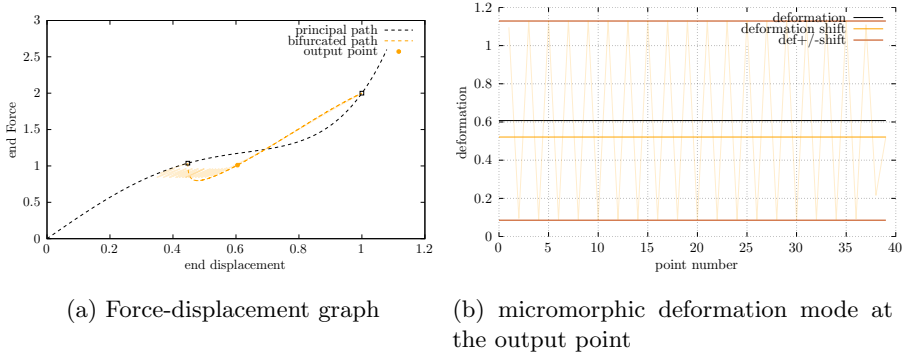


Fig. 8: End force-displacement graphs with principal path in black and first bifurcated branch in orange for the case where the short wavelength instability appears first along the principal path. Empty square marks represent the location of the bifurcation points. In transparent plain orange line is displayed the results on the discrete model for comparison. (a) Results using the micromorphic equivalent medium. (b) Values of deformation and deformation shift for the micromorphic model at the output point of the force-displacement graph and comparison with discrete results at the same point.

4.2 Long-wavelength instability and localization

Internal energy model parameter are chosen to be $K_1 = K_2 = N_2 = N_2 = 1$ and $M_1 = -1$, $M_2 = 3$ so that the system should display a long-wavelength instability followed by a localization, as explained in the discrete analysis section.

Results corresponding to the numerical computation of the problem on the discrete system are displayed in Fig.9. The systems shows a non-monotonic up-down-up principal branch (Fig.9a) in plain black line which comes to a limit point at $(\Delta_\epsilon, F) = (0.525731, 0.9711368291)$. According to [17], the up-down-up behavior ensures a localization phenomenon appearing after the first turning point. A series of very close bifurcation points appear indeed right after the turning point. The first bifurcation point corresponds to $(\Delta_\epsilon, F) = (0.525852, 0.9711376579)$. From that point, a bifurcated branch in plain green line emerges that an almost horizontal line (called the Maxwell line [26]). This branch appears to be unstable and actually contains oscillations (see the zoom in Fig.9b corresponding to propagation of the localized mode across the springs (Fig.9c) to finally reach almost the entire length of the system Fig.9d. The predicted long-wavelength instability followed by a localization is thus confirmed. Author would like to emphasize that the more springs are present in the system, the smaller are the amplitudes of the observed oscillations but this amplitude also depends on the system's stiffness parameters (K_i, M_i, N_i $i = 1, 2$). This oscillating feature has been observed also experimentally and

numerically in the literature [27, 28]. The localization starts at one end of the system due to imperfect boundary conditions that break the periodicity.

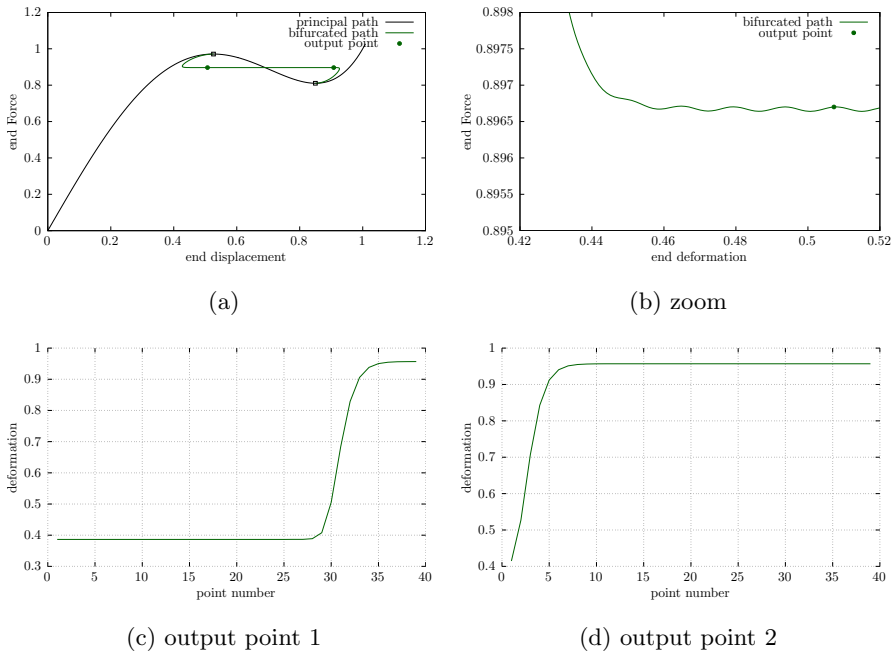


Fig. 9: Numerical results of computation on the discrete system where the long wavelength instability appears first along the principal path. (a) End force-displacement graph with principal path in black and first bifurcated branch in green. Empty squares mark the location of bifurcation points and the plain circles the computation points for which bifurcated modes are outputted. (b) and (c) bifurcation modes represented in terms of deformation corresponding to the plain circle output points.

When using the micromorphic equivalent medium, the principal path is appropriately captured and the limit point corresponds to point $(\Delta_E, F) = (0.525731, 0.9711376579)$ with relative error of the order of magnitude of the computer's accuracy on both displacement and force values. No bifurcation point is detected after the limit point using a perfect system. As a consequence the localization phenomenon cannot be captured this way. Using an imperfection of 0.1% on the stiffness of the first element, the beginning of the discrete bifurcation branch is captured but the plateau cannot be reached. Additionally, no bifurcation point can be identified because of imperfection. The point where the imperfect curve diverges from the perfect one happens for $(\Delta_E, F) = (0.511623, 0.9704268022)$, with relative error of $2.7 \cdot 10^{-2}$ on the displacement and $7 \cdot 10^{-4}$ on the force value. Modifying the imperfection

amplitude leads to a modification of the point of divergence from the principal path whereas changing the number of elements in the computation implies a change in the proximity of the branch to the principal path. As so, a higher number of elements leads to a branch closer to the principal path and a larger imperfection leads to an increasing values for the divergence point displacement-force couple. Finally, when the value of the deformation and deformation shift across the elements is plotted, the localized mode does not appear. The micromorphic medium seems to lack, in essence, the ability to appropriately capture localization as it can capture the onset, if imperfections are introduced, but cannot reproduce the Maxwell line behavior.

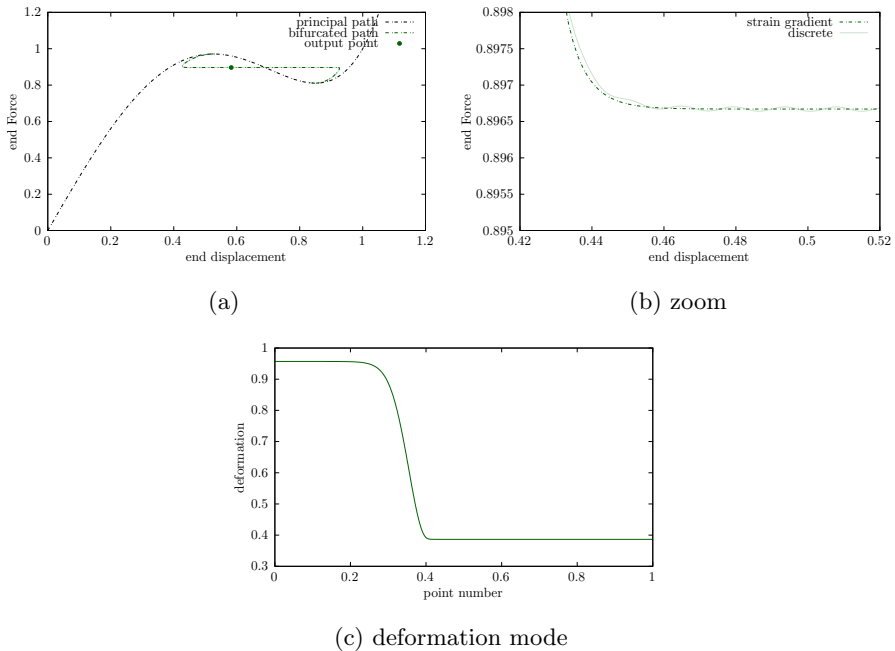


Fig. 10: End force-displacement graphs for computations using the strain-gradient equivalent medium for the case where the long wavelength instability appears first along the principal path. (b) zoom at the beginning of the horizontal part of bifurcated branch (c) strain-gradient deformation mode at output point of graph Fig.10a

When using the strain-gradient equivalent medium, the principal path is appropriately captured with a limit point located at $(\Delta_E, F) = (0.525731, 0.9711376579)$ with relative error of the order of magnitude of the computer's accuracy on both displacement and force values. Right after this limit point, a bifurcation point is detected at point

$(\Delta_E, F) = (0.5262165, 0.9711368274)$ with relative error of 7.10^{-4} on the displacement and of the order of magnitude of the computer's accuracy on the force value. The subsequent unstable bifurcating branch seems to be in very good agreement with the reference discrete branch but does not display any oscillations (cf. Fig.10a and Fig.10b). The associated deformation mode corresponds to a localization propagating along the system's length with values agreeing with those of the discrete model (cf. Fig.10c). It can thus be concluded that the strain gradient model is able to capture in a satisfactory manner the localization behavior and reproduces accurately the Maxwell line but not the oscillations appearing along this line.

From this second numerical study of a long-wavelength bifurcating system, it appears that both models are able to capture the limit point accurately but only the strain-gradient model can capture the bifurcation point and subsequent localization that appear afterwards. An imperfect micromorphic model has been proposed to try to capture the bifurcated branch. This model could propose an equilibrium path that is different from the perfect principal path but this path does not corresponds to the discrete bifurcated branch and especially fails to capture the Maxwell line. This second numerical study is of great importance as it shows the benefits of using strain-gradient equivalent medium when localization phenomena are to be modeled.

5 Conclusion

The objective of this paper is to question the ability of two families of generalized continua (namely micromorphic or strain-gradient) in capturing appropriately onset and post-bifurcated behavior of systems displaying either a patterning type of bifurcation (meaning short-wavelength instability) or a localization phenomenon following a long-wavelength instability. To allow for an analytical treatment of the problem, the studied system is an assembly of non-linear springs attached to direct and next-to-neighbor nodes and with stiffness parameters adjusted to display one or the other type of instability. The equivalent media energy are built analytically by microscopic analysis for the micromorphic medium or by Taylor expansion for the strain-gradient medium. A numerical study has been carried out to compare quantitatively the results with a reference computation on a discrete system and to study the ability of both models to capture post-bifurcated localization behavior. It appears that the micromorphic equivalent medium is the only one able to appropriately capture the onset and the post-bifurcation equilibrium path when a short-wavelength instability appears, creating a pattern of deformation, while the strain-gradient equivalent medium is the only one able to appropriately capture the localization phenomenon appearing after a long-wavelength instability. This study, on a simple system, allows us to build analytically tractable models and thus avoid errors stemming from numerical approximations. Moreover, the conclusions drawn out in this paper explain the choice made by [19] to

use a micromorphic model at the macroscopic scale in their numerical homogenization.

Of course, the two types of models compared in this study could be combined and this is the authors recommendation if both localization and patterning are expected to happen in the modeled system. This idea is currently under investigation, along with studying the ability of each model to capture non-commensurate instabilities that would appear if more complex models are used, as suggested in [18]. The case of a post-bifurcated branch corresponding to a global first instability that is supercritical in both load and displacement and hence does not lead to localization should also be investigated as it appears to be possible (cf. [29]). Finally, an extension of this study to two-dimensional or three-dimensional examples, as proposed in [30] is currently studied.

Declarations

Acknowledgements

This work was supported by the Agence Nationale de la Recherche (ANR) Project MAX-OASIS ANR-19-CE08-0005, the Center of Research of Ecoles de Saint-Cyr Coëtquidan (CREC) at the Military Academy of Saint-Cyr Coëtquidan and the Institut de Recherche Dupuy de Lôme at University of Bretagne Sud. The author also would like to thank professors N. Triantafyllidis and S. Neukirch for their advices and fruitful discussions and professor R.S.Elliott for his scientific guidance and help with numerical implementations.

Conflicts of Interest/Competing Interests

The author states that there is no conflict of interest.

References

- [1] Brechet, Y., Embury, J.D.: Architected materials: Expanding materials space. *Scripta Materialia* **68**(1), 1–3 (2013)
- [2] Barthelat, F.: Architected materials in engineering and biology: fabrication, structure, mechanics and performance. *International Materials Reviews* **60**(8), 413–430 (2015)
- [3] Poncelet, M., Somera, A., Morel, C., Jailin, C., Auffray, N.: An experimental evidence of the failure of Cauchy elasticity for the overall modeling of a non-centro-symmetric lattice under static loading. *International Journal of Solids and Structures* **147**, 223–237 (2018)
- [4] Combescure, C., Elliott, R.S., Triantafyllidis, N.: Deformation patterns and their stability in finitely strained circular cell honeycombs. *Journal of the Mechanics and Physics of Solids*, 103976 (2020)
- [5] He, Y., Zhou, Y., Liu, Z., Liew, K.M.: Buckling and pattern transformation of modified periodic lattice structures. *Extrem. Mech. Lett.* **22**, 112–121 (2018)
- [6] Papka, S.D., Kyriakides, S.: Biaxial crushing of honeycombs: —part 1: Experiments. *International Journal of Solids and Structures* **36**(29), 4367–4396 (1999)
- [7] Toupin, R.: Elastic materials with couple-stresses. *Archive for rational mechanics and analysis* **11**(1), 385–414 (1962)
- [8] Mindlin, R.: Micro-structure in linear elasticity, *archs. ration mech. Analysis* **1**(4), 16 (1964)
- [9] Mindlin, R.D.: Second gradient of strain and surface-tension in linear elasticity. *International Journal of Solids and Structures* **1**(4), 417–438 (1965)
- [10] Eringen, A.: Linear theory of micropolar elasticity [m]. *J. elasticity. J. Math. Mech* **15**, 909 (1966)
- [11] Mindlin, R.D., Eshel, N.: On first strain-gradient theories in linear elasticity. *International Journal of Solids and Structures* **4**(1), 109–124 (1968)
- [12] Auffray, N., Dirrenberger, J., Rosi, G.: A complete description of bi-dimensional anisotropic strain-gradient elasticity. *International Journal of Solids and Structures* **69**, 195–206 (2015)
- [13] Cosserat, E., Cosserat, F.: Théorie des corps déformables. *Bull. Am. Math.*

Soc. **19**(1913), 242–246 (1913)

- [14] Green, A., Rivlin, R.: Multipolar continuum mechanics. *Archive for Rational Mechanics and Analysis* **17**(2), 113–147 (1964)
- [15] Mindlin, R.D.: Microstructure in linear elasticity. Technical report, Columbia Univ New York Dept of Civil Engineering and Engineering Mechanics (1963)
- [16] Koiter, W.: Couple-stress in the theory of elasticity. In: *Proc. K. Ned. Akad. Wet.*, vol. 67, pp. 17–44 (1964). North Holland Pub
- [17] Triantafyllidis, N., Bardenhagen, S.: On higher order gradient continuum theories in 1-D nonlinear elasticity. Derivation from and comparison to the corresponding discrete models. *J. Elast.* **33**(3), 259–293 (1993)
- [18] Truskinovsky, L., Vainchtein, A.: Quasicontinuum modelling of short-wave instabilities in crystal lattices. *Philos. Mag.* **85**(33-35), 4055–4065 (2005)
- [19] Rokoš, O., Ameen, M.M., Peerlings, R.H.J., Geers, M.G.D.: Micromorphic computational homogenization for mechanical metamaterials with patterning fluctuation fields. *J. Mech. Phys. Solids* **123**, 119–137 (2019)
- [20] Combescure, C., Henry, P., Elliott, R.S.: Post-bifurcation and stability of a finitely strained hexagonal honeycomb subjected to equi-biaxial in-plane loading. *International Journal of Solids and Structures* **88**, 296–318 (2016)
- [21] Combescure, C., Elliott, R.S.: Hierarchical honeycomb material design and optimization: Beyond linearized behavior. *International Journal of Solids and Structures* **115**, 161–169 (2017)
- [22] Ericksen, J.: *The cauchy and born hypotheses for crystals. Mechanics and mathematics of crystals: selected papers of JL Ericksen.* Singapore: World Scientific Publishing Co, 117–33 (2005)
- [23] Elliott, R.S., Shaw, J.A., Triantafyllidis, N.: Stability of thermally-induced martensitic transformations in bi-atomic crystals. *J. Mech. Phys. Solids* **50**(11), 2463–2493 (2002)
- [24] Elliott, R.S.: Multiscale bifurcation and stability of multilattices. *J. Comput. Mater. Des.* **14**(SUPPL. 1), 143–157 (2007)
- [25] Doedel, E.J., Champneys, A.R., Dercole, F., Fairgrieve, T.F., Kuznetsov, Y.A., Oldeman, B., Paffenroth, R., Sandstede, B., Wang, X., Zhang, C.: *Auto-07p: Continuation and bifurcation software for ordinary differential equations* (2007)

- [26] Le, K.: Introduction to micromechanics: Classical and quantum mechanics. Nova Science, New York (2011)
- [27] Forest, S., Blazy, J.S., Chastel, Y., Moussy, F.: Continuum modeling of strain localization phenomena in metallic foams. *J. Mater. Sci.* **40**(22), 5903–5910 (2005)
- [28] Findeisen, C., Forest, S., Hohe, J., Gumbsch, P.: Discrete and continuum modelling of size effects in architected unstable metamaterials. *Contin. Mech. Thermodyn.* **32**(6), 1629–1645 (2020)
- [29] Santisi d’Avila, M.P., Triantafyllidis, N., Wen, G.: Localization of deformation and loss of macroscopic ellipticity in microstructured solids. *J. Mech. Phys. Solids* **97**, 275–298 (2016)
- [30] Bardenhagen, S., Triantafyllidis, N.: Derivation of higher order gradient continuum theories in 2,3-d non-linear elasticity from periodic lattice models. *J. Mech. Phys. Solids* **42**(1), 111–139 (1994)